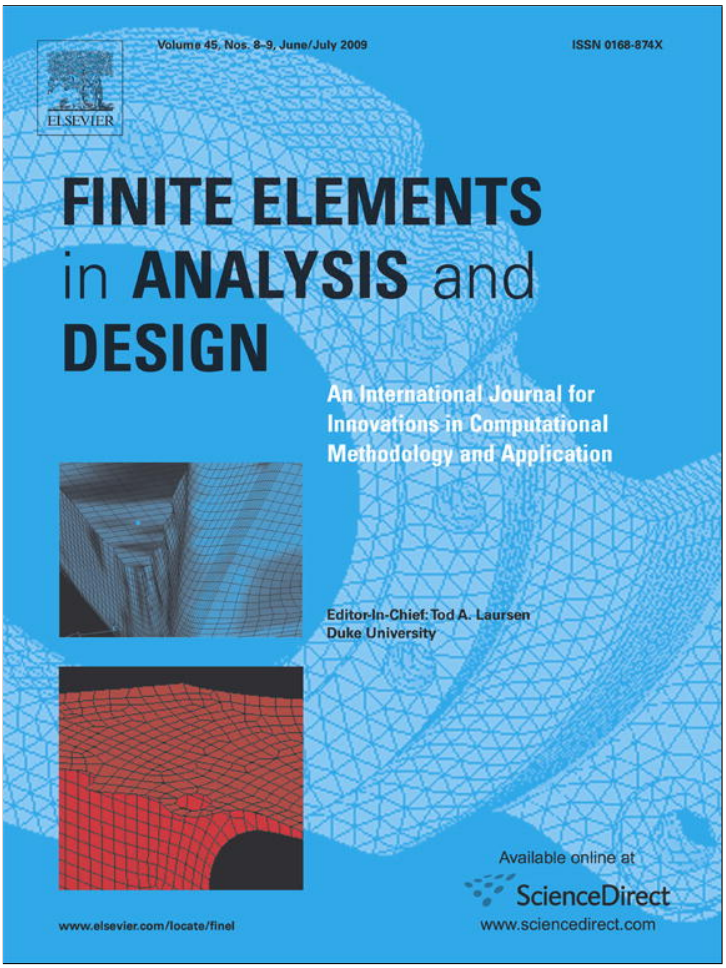

Finite Elements in Analysis and Design 45 (2009) 583 – 591

Contents lists available at ScienceDirect

Finite Elements in Analysis and Design

journal homepage: www.elsevier.com/locate/finel

Analysis of a continuum-based beam element in the framework of explicit-FEM

J.L. Curiel Sosa[a,*], A.J. Gil[b]

[a]Departament de Matemàtica Aplicada III (MA3), Laboratori de Càlcul Numèric (LaCàN), Escola Tècnica Superior d'Enginyers de Camins, Canals i Ports de Barcelona (ETSECCPB), Universitat Politècnica de Catalunya (UPC), C. Nord, Edif C2, Jordi Girona 1, 08034 Barcelona, Spain
[b]Civil and Computational Engineering Centre, Swansea University, Singleton Park, Swansea SA2 8PP, UK

ARTICLE INFO

Article history:
Received 17 May 2008
Received in revised form 24 March 2009
Accepted 24 March 2009
Available online 23 April 2009

Keywords:
Continuum-based (CB) beam element
Finite element analysis
Explicit dynamic analysis

ABSTRACT

In this paper, a continuum-based (CB) beam element based on the original work of Belytschko [Nonlinear Finite Elements for Continua and Structures, Wiley, New York, 2001] has been modified and analysed in the framework of explicit finite element methods. Two main differences are introduced with respect to the original finite element technology proposed in Belytschko [Nonlinear Finite Elements for Continua and Structures, Wiley, New York, 2001]. Firstly, the velocity gradient tensor is computed in the slave nodes of the finite element rather than in the master nodes, enabling a more effective computational performance in terms of CPU-time as well as convergence. Secondly, the thickness of the element is assumed to be variable, which allows dilation and/or contraction when large deformation processes are involved. A series of numerical examples are presented in order to verify the robustness and capabilities of the algorithm.

1. Introduction

Within the finite element modelling of long thin structures, three main strategies may be outlined depending upon the derivation of the finite element employed for the numerical simulation [2,3]. The first strategy is based upon the use of continuum elements. However, this approach requires a large number of these elements, resulting in increased computational cost. Moreover, modelling of long thin structures with continuum elements also leads to a poor conditioning of the resulting semidiscretised system of equations which could lead to a lack of stability and/or lack of accuracy in the results [1].

Another approach for the modelling of long thin structural elements is based upon the use of classical beam elements [4–6]. In these elements, assumptions verified through experimentation are imposed on the kinematics and kinetics of the problem with the purpose of representing more realistically the physical response of the structural element. However, in the case of explicit simulations, the use of classical beam elements leads to a severely restricted critical time step and therefore a prohibitively high computational cost. For instance, a Timoshenko beam element decreases stability if the rotational mass is predetermined to vanish. However, it should be mentioned that this stability—for the Timoshenko beam—is not sensibly affected if the inertial contributions of rotations and shear are adequately selected in a block diagonal mass matrix.

A third approach, widely used nowadays, is the continuum-based (CB) beam element [1,7] approach where, by starting from a continuum formulation, structural assumptions are imposed in order to feasibly represent the behaviour of standard beam structural elements. The CB approach is simpler and provides an attractive framework given the discretisation approach undertaken than classical theories such as Timoshenko beam theory, see Ref. [1]. This third strategy yields excellent results and will thus be used in this paper. Composite elements are allowed provided that through layers we can have different materials.

In this paper, following previous work in Ref. [8], an effective treatment of finite strains developed under shear stress conditions has been implemented for CB elements. In particular, the kinematics of the rotating cross-section is based on the introduction of directors. A similar corotational formulation for two-dimensional beam elements is presented in [9], where the Hellinger–Reissner variational principle is used under an implicit framework, which requires the computation of a tangent modulus.

Shear locking is a further important consideration when beam elements are to be studied in the context of thin long structures, see [10]. Using a Timoshenko finite element with interdependent shape functions for shear and bending, Ref. [11] circumvents shear locking. Meanwhile, Ref. [5] proposes a formulation based upon Hamilton's Principle [12]. In this work, the technique of selective-reduced integration, as used in [1,13], is employed to prevent shear locking. Also, in [10] the shear locking behaviour in an isoparametric curved beam element is avoided by means of reduced integration. Other techniques such as mixed interpolation schemes are proposed to solve the shear locking problem, see [14].

* Corresponding author. Tel.: +34 934017315; fax: +34 934011825.
E-mail addresses: jose.luis.curiel@upc.edu, jlcurie@yahoo.es (J.L. Curiel Sosa).

0168-874X/$ - see front matter © 2009 Elsevier B.V. All rights reserved.
doi:10.1016/j.finel.2009.03.003

In this paper, an explicit corotational formulation for a CB beam element based upon a continuum rectangular element is presented. Further details related to corotational formulations applied to beam elements can be found in [15–17]. Two main improvements have been introduced with respect to the original element developed in [1]. Firstly, the velocity gradient tensor is computed in the slave nodes of the finite element rather than in the master nodes, enabling a more effective computational performance in terms of CPU-time as well as convergence. This is due to the fact that the critical time step is increased each time increment [18,19] and, hence, the condition for stability are less restrictive in the explicit scheme adopted. Secondly, the thickness of the element is assumed to be variable which allows dilation and/or contraction when large deformation processes are involved.

One of the main objectives of this CB element was its use in a subcycling algorithm. The master–slave decomposition of the CB element makes it suitable for the transmission of information in the interface when using subcycling algorithms. This is the case of a bar embedded into a surrounding continuum. A pullout test is included to show the performance of the CB element in a subcycling algorithm. No description of the subcycling algorithm used is included as it is out of the main scope of this paper.

The structure of the paper is outlined as follows. Firstly, the fundamentals of the formulation of the CB finite element are outlined in terms of kinematics and kinetics. Secondly, the explicit numerical scheme used for the computational simulations is briefly described. Thirdly, a brief description of the implemented computational algorithm is summarised. Fourthly, numerical examples are presented for the cases of tension, compression and bending. A final example is included to demonstrate the performance of this CB element when embedded into a surrounding continuum. Finally, some concluding remarks are made.

2. Continuum-based beam formulation

A CB element depicted in Fig. 1. The nodes at the top and bottom are called slave nodes. These define the continuum element. Master nodes are located in the intersection of the lines connecting slave nodes and the reference line—or mid-line. Each master node is connected to a couple of slave nodes. The structural system is composed of a discretisation of CB beam elements, *nmast* being the total number of master nodes and 2*nmast* the total number of slave nodes. The semidiscretised momentum equations are formulated at the master nodes, i.e. the unknowns of the problem are taken to be the degrees of freedom at the master nodes. Moreover, for computational convenience, velocities at the master nodes are chosen as the primary unknowns, from which the displacements and rotations are deduced through the corresponding kinematic relationships. Meanwhile, the slave nodes are indirectly used for the computation of internal strains, stresses and thus, internal forces. The vector of unknown velocities at the master nodes is then given as

$$\mathbf{v} = [v_{x1} \;\; v_{y1} \;\; \dot{\theta}_1 \;\; \ldots \;\; v_{x\kappa} \;\; v_{y\kappa} \;\; \dot{\theta}_\kappa \;\; \ldots \;\; v_{x\,nmast} \;\; v_{y\,nmast} \;\; \dot{\theta}_{nmast}]^T \tag{1}$$

where it can be observed three degrees of freedom are considered per master node κ, namely the velocities $v_{x\kappa}$ and $v_{y\kappa}$ along with the rate of rotation $\dot{\theta}_\kappa$ of the cross-section around the master node. Hereafter, subscript κ will be used to denote a master node, whilst κ^- and κ^+ denote the corresponding slave nodes located below and above the master node as depicted in Fig. 1. It is important to emphasise that only the degrees of freedom corresponding to velocities/displacements will be considered when referring to slave nodes, see Fig. 1.

2.1. Kinematics

Every CB element is defined in terms of fibres and laminae. As illustrated in Fig. 1 fibres are imagined to span from slave node κ^- to slave node κ^+ passing through the master node κ. Laminae link adjacent master nodes or adjacent slave nodes, where the lamina linking the master nodes of an element defines the so-called mid-line of the element. The kinematic description of the structural system is based upon the definition of the so-called directors $\mathbf{p}_\kappa$, unit vectors always aligned with the fibres of the CB element [20,8]. This enables the accurate computation of finite strains developed under the action of shear stresses. The vector of unknowns particularised for a master node κ is given as

$$\mathbf{v}_\kappa = [v_{x\kappa} \;\; v_{y\kappa} \;\; \dot{\theta}_\kappa]^T \tag{2}$$

The angle of rotation θ_κ defines the orientation of the director $\mathbf{p}_\kappa$. It is important to note that the director is not necessarily perpendicular to the mid-line formed by the master nodes. Thus, at a master node κ the time dependent director $\mathbf{p}_\kappa$ can be formulated as

$$\mathbf{p}_\kappa = \cos\theta_\kappa \mathbf{e}_x + \sin\theta_\kappa \mathbf{e}_y \tag{3}$$

where $\{\mathbf{e}_x, \mathbf{e}_y\}$ represent the standard Euclidean two-dimensional base. The coordinates of the slave nodes are readily calculated given the position of the master node $\mathbf{x}_\kappa$ and the director $\mathbf{p}_\kappa$ as

$$\mathbf{x}_{\kappa^+} = \mathbf{x}_\kappa + \tfrac{1}{2} h_\kappa \mathbf{p}_\kappa, \quad \mathbf{x}_{\kappa^-} = \mathbf{x}_\kappa - \tfrac{1}{2} h_\kappa \mathbf{p}_\kappa \tag{4}$$

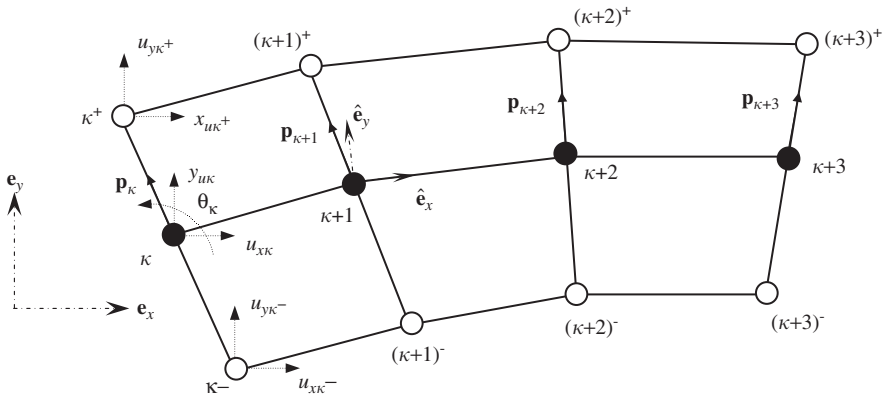

Fig. 1. The figure shows a typical continuum-based (CB) element. In this sample, it is composed of four master nodes—in bold—and eight slave nodes but other configurations are also possible.

where h_κ represents the thickness of the CB element at the master node κ which may vary throughout the loading process. Thus, the velocities at the slave nodes are computed as

$$\mathbf{v}_{\kappa^+} = \mathbf{v}_\kappa + \tfrac{1}{2} h_\kappa \boldsymbol{\Omega}_\kappa \times \mathbf{p}_\kappa, \quad \mathbf{v}_{\kappa^-} = \mathbf{v}_\kappa - \tfrac{1}{2} h_\kappa \boldsymbol{\Omega}_\kappa \times \mathbf{p}_\kappa \tag{5}$$

where $\times$ denotes the standard cross-product vector and $\boldsymbol{\Omega}_\kappa$ represents the angular velocity vector at the master node κ and is defined as

$$\boldsymbol{\Omega}_\kappa = \frac{D\theta_\kappa}{Dt}\mathbf{e}_z, \quad \mathbf{e}_z = \mathbf{e}_x \times \mathbf{e}_y \tag{6}$$

designating D/Dt the standard material or Lagrangian time derivative. A corotational basis $\{\hat{\mathbf{e}}_x, \hat{\mathbf{e}}_y\}$ may be defined at any point within the element which is aligned such that the unit vector $\hat{\mathbf{e}}_x$ is always tangential to the lamina at that point. Observe that as fibres and laminae rotate independently, the rotation of the director $\mathbf{p}_\kappa$ represented by θ_κ will not be equal to the rotation of the corotational basis vector $\hat{\mathbf{e}}_x$. Defining the parent coordinates of the CB element as ξ and η, the corotational basis $\{\hat{\mathbf{e}}_x, \hat{\mathbf{e}}_y\}$ at any point within the element can be expressed in terms of the Euclidean basis $\{\mathbf{e}_x, \mathbf{e}_y\}$ as follows:

$$\begin{bmatrix} \hat{\mathbf{e}}_x \\ \hat{\mathbf{e}}_y \end{bmatrix} = \begin{bmatrix} \frac{x_{,\xi}}{\sqrt{x_{,\xi}^2+y_{,\xi}^2}} & \frac{y_{,\xi}}{\sqrt{x_{,\xi}^2+y_{,\xi}^2}} \\ \frac{-y_{,\xi}}{\sqrt{x_{,\xi}^2+y_{,\xi}^2}} & \frac{x_{,\xi}}{\sqrt{x_{,\xi}^2+y_{,\xi}^2}} \end{bmatrix} \begin{bmatrix} \mathbf{e}_x \\ \mathbf{e}_y \end{bmatrix} \tag{7}$$

where $x_{,\xi}$ and $y_{,\xi}$ represent the derivatives of the current coordinates x and y of the considered point with respect to the corresponding parent coordinate ξ. According to a finite element spatial semidiscretisation, the coordinates of any point within the CB element can be expanded in terms of the coordinates of the corresponding slave nodes as follows:

$$\mathbf{x} = \sum_{\kappa^*=1}^{nslave} \mathbf{x}_{\kappa^*} N_{\kappa^*}(\xi, \eta) \tag{8}$$

where for the sake of convenience a new subscript κ^* has been introduced to represent all the slave nodes within a single CB element, *nslave* denotes the total number of slave nodes within the CB element and where N_{κ^*} represents the shape function corresponding to the slave node κ^*. The Jacobian tensor $\mathbf{J}_\xi$ representing the transformation between the parent domain and the current domain is given by

$$\mathbf{J}_\xi = \begin{bmatrix} x_{,\xi} & x_{,\eta} \\ y_{,\xi} & y_{,\eta} \end{bmatrix} \tag{9}$$

which is expanded according to a finite element spatial semidiscretisation as

$$\mathbf{J}_\xi = \sum_{\kappa^*=1}^{nslave} \mathbf{x}_{\kappa^*} \otimes N_{\kappa^*,\boldsymbol{\xi}}, \quad N_{\kappa^*,\boldsymbol{\xi}} = [N_{\kappa^*,\xi} \;\; N_{\kappa^*,\eta}]^T \tag{10}$$

An orthogonal matrix $\mathbf{R}$ representing the rotation between the Euclidean basis $\{\mathbf{e}_x, \mathbf{e}_y\}$ and the corotational basis $\{\hat{\mathbf{e}}_x, \hat{\mathbf{e}}_y\}$ can be defined as

$$\mathbf{R} = \begin{bmatrix} \mathbf{e}_x \cdot \hat{\mathbf{e}}_x & \mathbf{e}_x \cdot \hat{\mathbf{e}}_y \\ \mathbf{e}_y \cdot \hat{\mathbf{e}}_x & \mathbf{e}_y \cdot \hat{\mathbf{e}}_y \end{bmatrix} \tag{11}$$

Thus, the velocity $\mathbf{v}_{\kappa^*}$ of a slave node κ^* expressed with respect to the corotational basis, denoted $\hat{\mathbf{v}}_{\kappa^*}$, can be formulated as

$$\hat{\mathbf{v}}_{\kappa^*} = \mathbf{R}^T \mathbf{v}_{\kappa^*}, \quad \mathbf{v}_{\kappa^*} = [v_{x\kappa^*} \;\; v_{y\kappa^*}]^T, \quad \hat{\mathbf{v}}_{\kappa^*} = [\hat{v}_{\hat{x}\kappa^*} \;\; \hat{v}_{\hat{y}\kappa^*}]^T \tag{12}$$

Note that in comparison to the master node κ shown in Eq. (2), the number of degrees of freedom at a slave node κ^* is reduced to two.

The Jacobian tensor $\mathbf{J}_\xi$ can also be re-expressed in the corotational basis, denoted as $\hat{\mathbf{J}}_\xi$, as follows:

$$\hat{\mathbf{J}}_\xi = \mathbf{R}^T \mathbf{J}_\xi \mathbf{R}, \quad \hat{\mathbf{J}}_\xi = \begin{bmatrix} \hat{x}_{,\xi} & \hat{x}_{,\eta} \\ \hat{y}_{,\xi} & \hat{y}_{,\eta} \end{bmatrix} \tag{13}$$

Moreover, the gradient of the shape functions expressed in the corotational basis, which will be required for implementation purposes, can be obtained by means of the chain rule as

$$N_{\kappa^*,\hat{\mathbf{x}}} = \hat{\mathbf{J}}_\xi^{-T} N_{\kappa^*,\boldsymbol{\xi}}, \quad N_{\kappa^*,\hat{\mathbf{x}}} = [N_{\kappa^*,\hat{x}} \;\; N_{\kappa^*,\hat{y}}]^T \tag{14}$$

In this way, the velocity gradient tensor expressed with respect to the corrotational basis, denoted $\hat{\mathbf{L}}$, can be given by

$$\hat{\mathbf{L}} = \sum_{\kappa^*=1}^{nslave} \hat{\mathbf{v}}_{\kappa^*} \otimes N_{\kappa^*,\hat{\mathbf{x}}}, \quad \hat{\mathbf{L}} = \begin{bmatrix} \hat{v}_{\hat{x},\hat{x}} & \hat{v}_{\hat{x},\hat{y}} \\ \hat{v}_{\hat{y},\hat{x}} & \hat{v}_{\hat{y},\hat{y}} \end{bmatrix} \tag{15}$$

For the particular case of the CB element presented in this paper, which is composed of four master nodes, Eq. (15) can be re-written in a compact matrix form as follows:

$$\begin{bmatrix} \hat{L}_{\hat{x}\hat{x}} & \hat{L}_{\hat{x}\hat{y}} \\ \hat{L}_{\hat{y}\hat{x}} & \hat{L}_{\hat{y}\hat{y}} \end{bmatrix} = \begin{bmatrix} \hat{v}_{\hat{x}1^*} & \hat{v}_{\hat{x}2^*} & \hat{v}_{\hat{x}3^*} & \hat{v}_{\hat{x}4^*} \\ \hat{v}_{\hat{y}1^*} & \hat{v}_{\hat{y}2^*} & \hat{v}_{\hat{y}3^*} & \hat{v}_{\hat{y}4^*} \end{bmatrix} \begin{bmatrix} N_{1^*,\hat{x}} & N_{1^*,\hat{y}} \\ N_{2^*,\hat{x}} & N_{2^*,\hat{y}} \\ N_{3^*,\hat{x}} & N_{3^*,\hat{y}} \\ N_{4^*,\hat{x}} & N_{4^*,\hat{y}} \end{bmatrix} \tag{16}$$

Finally, the rate of deformation tensor $\hat{\mathbf{D}}$ expressed with respect to the corotational basis can be deduced in a standard manner as

$$\hat{\mathbf{D}} = \tfrac{1}{2}(\hat{\mathbf{L}} + \hat{\mathbf{L}}^T) \tag{17}$$

2.2. Kinetics

Once the rate of deformation tensor $\hat{\mathbf{D}}$ has been calculated, the rate of the corotational Cauchy stress tensor $D\hat{\boldsymbol{\sigma}}/Dt$ [21], assuming elasticity, can be deduced as

$$\frac{D\hat{\boldsymbol{\sigma}}}{Dt} = \Xi(\hat{\mathbf{D}}) \tag{18}$$

As the corotational Cauchy stress tensor is frame-invariant, it can be expressed directly in terms of the corotational rate of deformation $\hat{\mathbf{D}}$ for a given constitutive law symbolised by Ξ. Thus, the internal forces at a slave node κ^*, denoted by $\mathbf{f}_{\kappa^*}$, can be obtained by integrating over the corresponding structural volume Ω as

$$\mathbf{f}_{\kappa^*}^{int} = \int_\Omega \mathbf{R}\hat{\boldsymbol{\sigma}} N_{\kappa^*,\hat{\mathbf{x}}} \, d\Omega, \quad \mathbf{f}_{\kappa^*}^{int} = [f_{x\kappa^*}^{int} \;\; f_{y\kappa^*}^{int}]^T \tag{19}$$

A selective-reduced integration is performed to avoid shear locking [13]. The quadrature points for the numerical integration can be placed through the thickness of the structural beam element if required for correct simulation of the problem. Once the internal forces $\mathbf{f}_{\kappa^*}^{int}$ have been obtained at every slave node κ^*, the corresponding internal forces $\mathbf{f}_\kappa^{int}$ at the master node κ can be deduced through the following transformation $\mathbf{T}$:

$$\mathbf{f}_\kappa^{int} = \mathbf{T}\mathbf{f}_{\kappa^*}^{int}, \quad \mathbf{f}_\kappa^{int} = [f_{x\kappa}^{int} \;\; f_{y\kappa}^{int} \;\; M_\kappa^{int}]^T \tag{20}$$

where $f_{x\kappa}^{int}$ and $f_{y\kappa}^{int}$ represent the internal forces at a master node κ and M_κ^{int} denotes the corresponding bending moment. The above

transformation equation (20) can be expanded for a particular master node κ in terms of its corresponding slave nodes κ^+ and κ^- as

$$\begin{bmatrix} f^{int}_{x\kappa} \\ f^{int}_{y\kappa} \\ M^{int}_{\kappa} \end{bmatrix} = \begin{bmatrix} 1 & 0 & 1 & 0 \\ 0 & 1 & 0 & 1 \\ (y_\kappa - y_{\kappa^-}) & (x_{\kappa^-} - x_\kappa) & (y_\kappa - y_{\kappa^+}) & (x_{\kappa^+} - x_\kappa) \end{bmatrix} \times \begin{bmatrix} f^{int}_{x\kappa^-} \\ f^{int}_{y\kappa^-} \\ f^{int}_{x\kappa^+} \\ f^{int}_{x\kappa^+} \end{bmatrix} \tag{21}$$

Analogously, external forces applied at slave nodes will be transformed into their counterparts at the master nodes, denoted by $\mathbf{f}^{ext}_{\kappa}$, by means of the transformation described above. This operation is updated at every time step to account for large rotations and/or deformations that could appear during the deformation process.

3. Explicit code algorithm

After performing the spatial semidiscretisation according to a finite element basis, the resulting system of second order in time dynamic equations can be given by

$$\mathbf{M}\mathbf{a}_n + \mathbf{C}\mathbf{v}_n + \mathbf{f}^{int}_n = \mathbf{f}^{ext}_n \tag{22}$$

where $\mathbf{M}$ represents the mass matrix, $\mathbf{C}$ denotes a damping matrix, $\mathbf{f}^{int}_n$ is the vector of internal forces dependent upon the displacement field $\mathbf{u}_n$ and $\mathbf{f}^{ext}_n$ is the vector of external forces at time level n. Vectors $\mathbf{a}_n$ and $\mathbf{v}_n$ stand for acceleration and velocity at time level n which, along with $\mathbf{u}_n$, are evaluated at the master nodes. In particular, the following central difference stencils are used for the approximation of the corresponding time derivatives:

$$\mathbf{v}_{n-1/2} = \frac{\mathbf{u}_n - \mathbf{u}_{n-1}}{\Delta t_{n-1/2}}, \quad \mathbf{a}_n = \frac{\mathbf{v}_{n+1/2} - \mathbf{v}_{n-1/2}}{\Delta t_n}, \quad \mathbf{v}_n = \frac{\mathbf{v}_{n+1/2} + \mathbf{v}_{n-1/2}}{2} \tag{23}$$

where Δt_n represents the incremental time step at time level n whilst the mid-time increments are given by

$$\Delta t_{n-1/2} = \frac{\Delta t_n + \Delta t_{n-1}}{2}, \quad \Delta t_{n+1/2} = \frac{\Delta t_{n+1} + \Delta t_n}{2} \tag{24}$$

In this paper, an adaptive time stepping scheme [18] has been used to overcome the limitations imposed by stability requirements of conventional fixed time stepping schemes. Substitution of Eqs. (23) into the system of dynamic equations (22) results in

$$[2\mathbf{M} + \Delta t_n \mathbf{C}]\mathbf{v}_{n+1/2} = [2\mathbf{M} - \Delta t_n \mathbf{C}]\mathbf{v}_{n-1/2} + [\mathbf{f}^{ext}_n - \mathbf{f}^{int}_n] \tag{25}$$

which enables the mid-time velocity $\mathbf{v}_{n+1/2}$, for diagonal mass and damping matrices, to be expressed in index notation as

$$v_{i,n+1/2} = \frac{2M_i - \Delta t_n C_i}{2M_i + \Delta t_n C_i} v_{i,n-1/2} + \frac{f^{ext}_{i,n} - f^{int}_{i,n}}{2M_i + \Delta t_n C_i} \tag{26}$$

Finally, the explicit algorithm is completed by computing the displacements at the time step $n+1$ according to the following updating formula:

$$\mathbf{u}_{n+1} = \mathbf{u}_n + \Delta t_{n+1/2} \mathbf{v}_{n+1/2} \tag{27}$$

In the simulations presented thereafter, the damping matrix $\mathbf{C}$ is computed according to the standard Rayleigh damping technique,

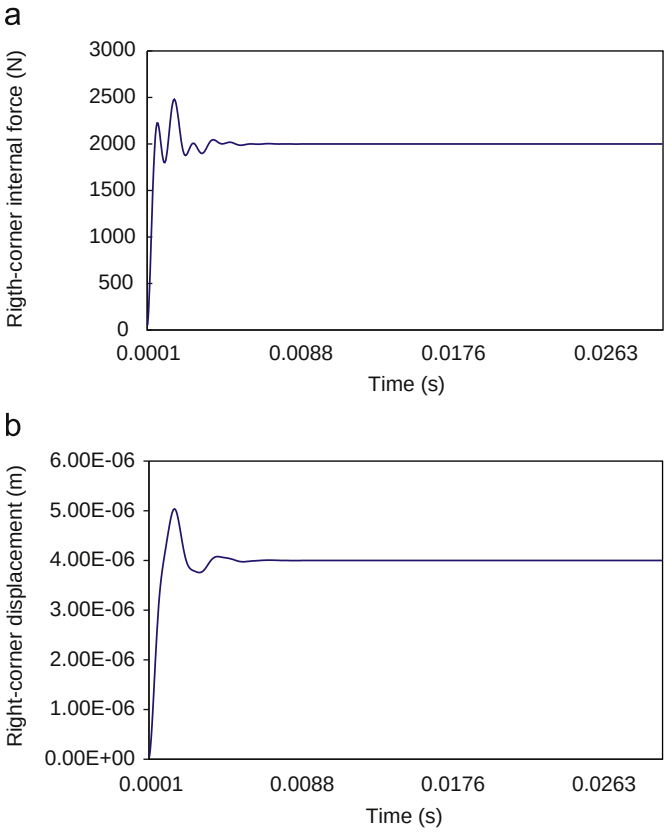

Fig. 2. Tension test: results at the master node corresponding to the external loading position: (a) internal force; (b) displacement.

such that $\mathbf{C}$ is proportional to the diagonalised mass matrix $\mathbf{M}$ in order to maintain the explicit form of the algorithm [18]. In index form this can be written as

$$C_i = 2\xi\omega_i M_i \tag{28}$$

where ξ is the selected damping ratio and ω_i symbolises the natural frequency of the master node at the degree of freedom considered. An alternative damping provided by Munjiza et al. [22], to damp a wider range of frequencies, combining stiffness and mass proportionality is implemented for problematic cases. The initiation of the scheme (26) requires knowledge of the velocity at time level $t_{-1/2}$. Thus, the following closure equation is considered:

$$\mathbf{v}_{-1/2} = -\mathbf{v}_{1/2} \tag{29}$$

The static solution may be obtained by attenuation of the transient response using an artificial damping technique. This would correspond to the steady state of the dynamic response. This is performed in this study by means of a dynamic relaxation strategy [23].

4. Computational algorithm

The computational algorithm is briefly outlined as follows:

(I) Extract velocities $\mathbf{v}_\kappa$ and displacements $\mathbf{u}_\kappa$ at master nodes.
(II) Update coordinates of master nodes $\mathbf{x}_\kappa$.
(III) Compute directors at master nodes $\mathbf{p}_\kappa$.
(IV) Compute velocities $\mathbf{v}_{\kappa^*}$ and coordinates $\mathbf{x}_{\kappa^*}$ of slave nodes.
(V) Compute internal forces at master nodes $\mathbf{f}^{int}_\kappa$.

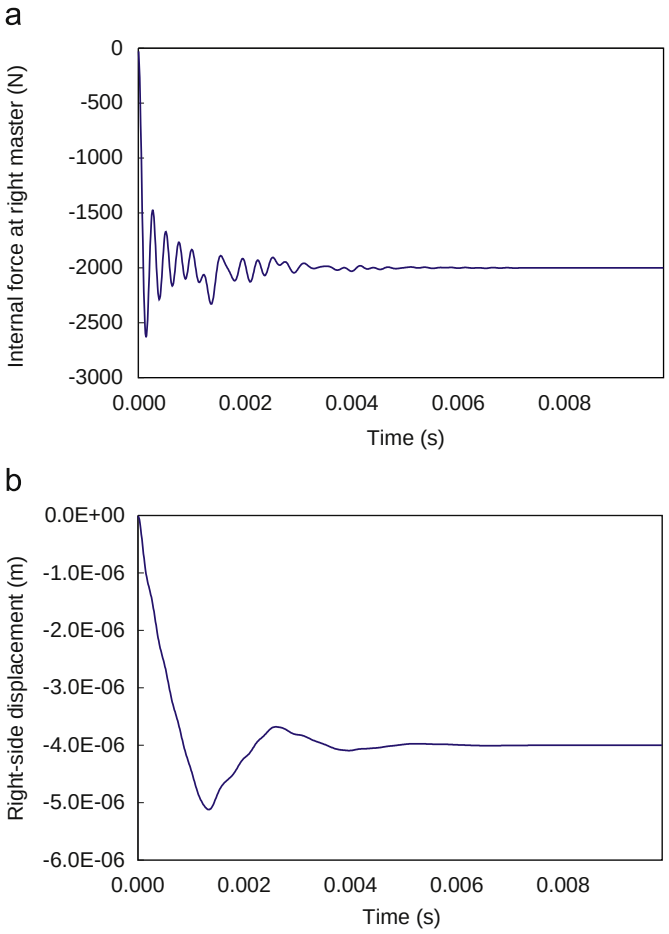

Fig. 3. Compression test: results at the master node corresponding to the external loading position: (a) internal force; (b) displacement.

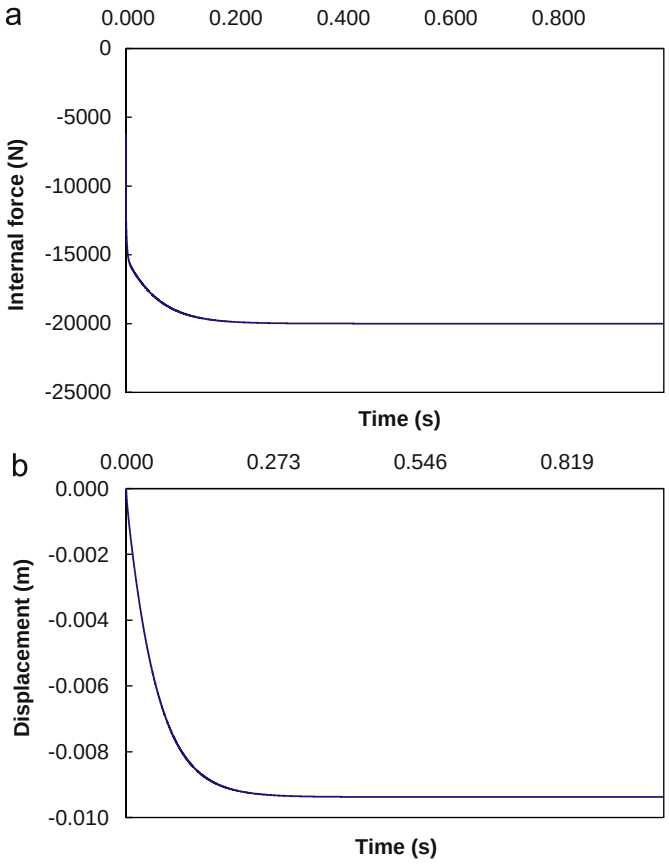

Fig. 4. Cantilever beam subjected to a tip load of 20 kN. Results at the master node corresponding to the external loading position: (a) internal force; (b) vertical displacement.

(VI) Compute external forces at master nodes $\mathbf{f}_{\kappa}^{ext}$.
(VII) Solve for velocities $\mathbf{v}_{\kappa}$ and displacements $\mathbf{u}_{\kappa}$ at master nodes.

In the above scheme, for the computation of the internal forces at master nodes gathered in step (V) above, the following algorithm is implemented:

(i) Define the corotational basis $\{\hat{\mathbf{e}}_x, \hat{\mathbf{e}}_y\}$, Eq. (7).
(ii) Compute Jacobian tensor $\mathbf{J}_{\xi}$, Eq. (10).
(iii) Obtain the rotation matrix $\mathbf{R}$, Eq. (11).
(iv) Obtain corotational velocities $\hat{\mathbf{v}}_{\kappa^*}$ and coordinates $\hat{\mathbf{x}}_{\kappa^*}$ at slave nodes, Eq. (12).
(v) Compute the corotational Jacobian tensor $\hat{\mathbf{J}}_{\xi}$, Eq. (13).
(vi) Compute gradient of the shape functions with respect to the corotational basis $N_{\kappa^*,\hat{\mathbf{x}}}$, Eq. (14).
(vii) Obtain the corotational velocity gradient tensor $\hat{\mathbf{L}}$, Eq. (15).
(viii) Obtain the corotational rate of deformation tensor $\hat{\mathbf{D}}$, Eq. (17).
(ix) Update the rate of stress tensor $\hat{\boldsymbol{\sigma}}$, Eq. (18).
(x) Compute contribution to internal force vector $\mathbf{f}_{\kappa^*}^{int}$ on slave nodes, Eq. (19).
(xi) Obtain contribution to internal force vector $\mathbf{f}_{\kappa}^{int}$ on master nodes, Eq. (20).

5. Numerical examples

For the numerical examples presented hereafter, a CB element with two master nodes and four slave nodes has been implemented.

5.1. Tension and compression tests

The tension and compression tests are simple, standard numerical tests applied here to assess the performance of the CB element formulation. A structural bar with dimensions 2 m × 1 m × 0.1 m is modelled by means of two CB elements with material parameters as follows: Young's modulus 1000 MPa, Poisson's ratio 0.3 and density 2700 kg/m^3.

A tensile force is applied at one edge of the structure to mimic the standard specimen pull-out test. An external force of 2 kN is distributed between the two slave nodes situated at the extreme edge of the element corresponding to the point of loading. Results displayed in Figs. 2(a) and (b) agree exactly with the analytical solution, which gives an elongation of 4×10^{-6} m with an axial stress of 20 kPa.

Similarly, a compressive force of 2 kN is applied to mimic the standard specimen compression test. In this case, a structural mesh of eight CB elements was utilised, whilst the geometry and material parameters remain as previously. Figs. 3(a) and (b) agree exactly with the analytical solution, which gives an elongation of -4×10^{-6} m with an axial stress of −20 kPa.

5.2. Cantilever beam

This example models a classical cantilever beam subjected to a lateral tip load. The structural cantilever with dimensions 1 m × 0.1 m × 0.1 m is modelled by means of eight CB elements with material parameters as follows: Young's modulus 71 000 MPa, Poisson's ratio 0.34 and density 2700 kg/m^3.

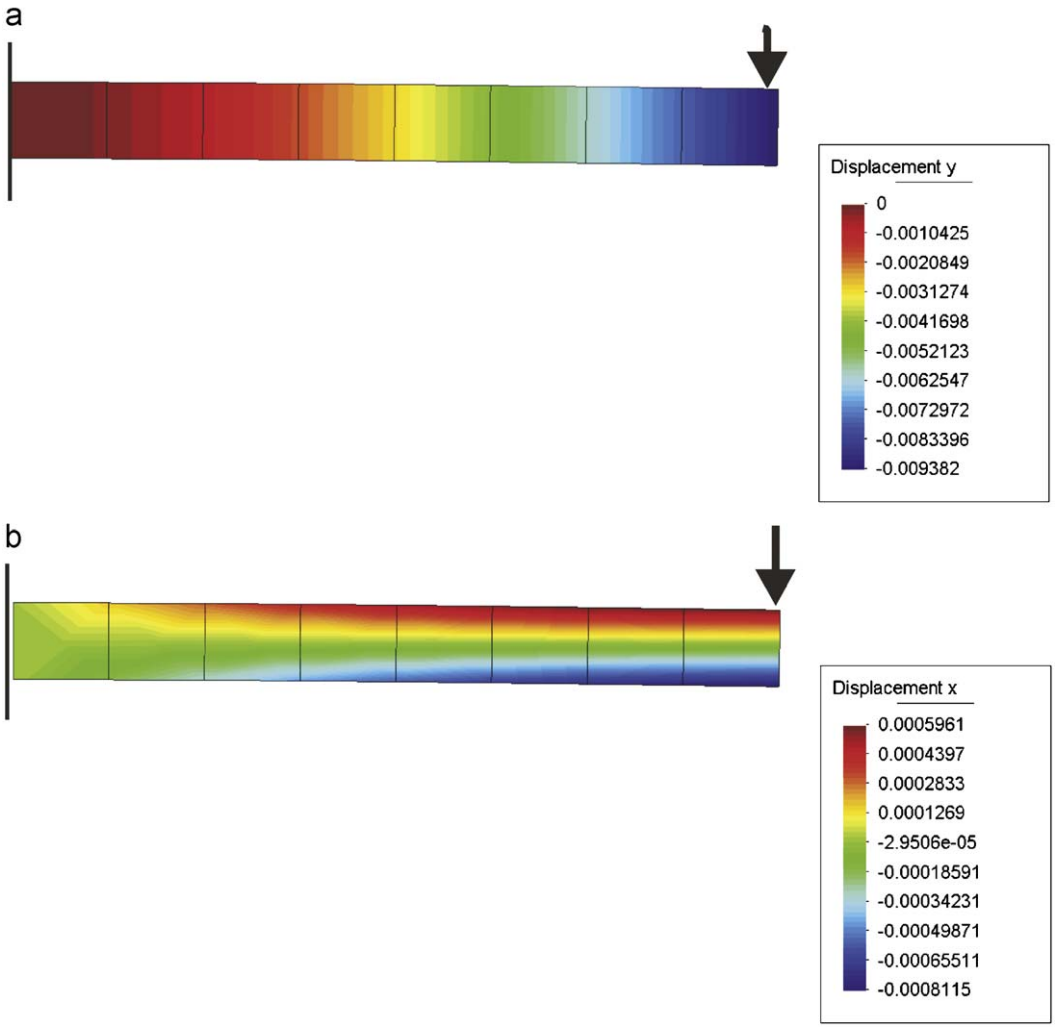

Fig. 5. Cantilever beam subjected to a tip load of 20 kN. Results at the master node corresponding to the external loading position: (a) vertical displacement (m); (b) horizontal displacement (m).

Firstly, an external force of 20 kN was divided between the two slave nodes situated at the extreme edge of the element corresponding to the point of loading. Applying selective-reduced integration over five quadrature points along the thickness of the element [1], results displayed in Figs. 4 and 5 for the master node corresponding to the position with maximum deflection, i.e. the free edge. The resulting deflection along the bar is compared with the analytical solution and the solution by Timoshenko elements in Fig. 7(a).

Secondly, an external force of 200 kN was applied in the same manner as above. Applying normal integration over nine quadrature points uniformly distributed through the element, results displayed in Fig. 6 for the master node agree. Comparisons with classical Timoshenko elements and with the analytical solution are provided in Fig. 7(b).

5.3. CB elements embedded into a surrounding continuum

In this numerical example, the simulation of a structural bar embedded in a surrounding medium is subjected to a pull-out force at one end. This test, represented in Fig. 8, models the behaviour of a standard steel reinforcement bar surrounded by a structural block of concrete. The concrete block is modelled with a mesh composed of 250 quadrilateral elements with four gauss points and thickness 78.5 mm. The nodes located on the boundary of the concrete block, indicated by the shaded area in Fig. 8 are fully fixed. The steel reinforcing bar consists of eight CB elements of cross-section area $\pi \times 10^{-4}$ m^2. Material properties are displayed in Table 1. The concrete block has been modelled by means of a plastic Mohr–Coulomb constitutive law in which friction and dilatancy angles coincide (associative flow). Details of the implementation of this constitutive law can be found in Appendix A following the proposed scheme by Simo and Taylor [24]. The steel reinforcing bar is subjected to a loading of 100 kN. The concrete block undergoes elongation caused by the axial deformation of the reinforcing bar at the interface, as can be observed in Fig. 9. For the numerical simulation, perfect bond is assumed between the steel and concrete components [25]. So the displacement in the steel bar are those form the surrounding concrete block. Displacement fields are shown in Fig. 9.

6. Conclusions

A continuum-based beam element based on the original work of Belytschko [1] was presented in this paper. Two improvements were introduced with respect to the original formulation. The velocity gradient tensor was computed in the slave nodes of the finite element rather than in the master nodes, enabling a more effective

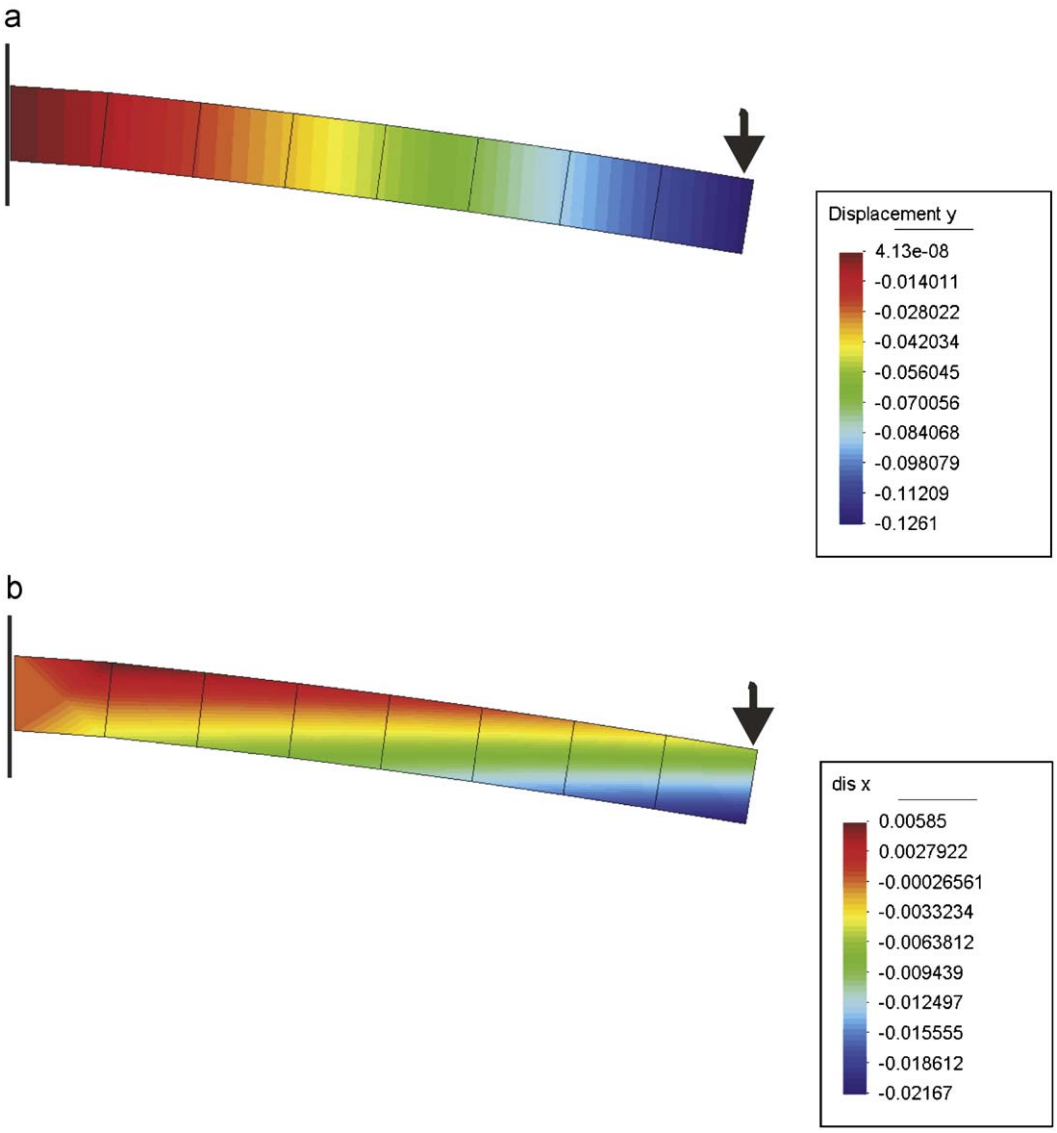

Fig. 6. Cantilever beam subjected to a tip load of 200 kN: results at the master node corresponding to the external loading position: (a) vertical displacement (m); (b) horizontal displacement (m).

computational performance in terms of CPU-time as well as convergence. Furthermore, the thickness of the element is assumed to be variable, which allows dilation and/or contraction when large deformation processes are involved. A series of numerical examples were shown to demonstrate the robustness and capabilities of the CB element.

Appendix A. Integration algorithm for the plastic Mohr–Coulomb material model

For the Mohr–Coulomb constitutive law, the yield surface can be expressed as the combination of principal stresses $\boldsymbol{\sigma}$ that define a pyramid with the apex located at the position which satisfies the condition $c = \cot\phi$ in the tensile side of the hydrostatic axis, where c is the cohesion and ϕ the angle of internal friction. The limited resistance in tension inherent within the Mohr–Coulomb constitutive law, enables a realistic representation of the concrete material. Each of the six planes representing the yielding pyramid is defined by means of the yielding function $\Phi_i(\boldsymbol{\sigma}, c, \phi) = 0$.

By considering an associative law, the yield function is adopted as the flow potential. The flow rule requires the consideration of singularities at the apex and at the intersections, or the so-called edges, of adjacent faces of the pyramid. Thus, plastic flow can be initiated at an edge, a face or at the apex of the yielding pyramid. In general, the flow rule for plastic evolution from a face predicts a plastic strain rate $\dot{\boldsymbol{\epsilon}}^p$ given by

$$\dot{\boldsymbol{\epsilon}}^p = \dot{\gamma}\mathbf{N}, \quad \mathbf{N} = \frac{\partial \Phi_i}{\partial \boldsymbol{\sigma}} \tag{30}$$

where $\mathbf{N}$ is a vector normal to the yielding surface defined by the plane $\Phi_i = 0$ and $\dot{\gamma}$ represents the plastic multiplier [26]. At the edges between two adjacent faces of the pyramid, the flow rule is then given by

$$\dot{\boldsymbol{\epsilon}}^p = \dot{\gamma}_a\mathbf{N}_a + \dot{\gamma}_b\mathbf{N}_b \tag{31}$$

where subscripts a and b stand for the adjacent faces of the pyramid represented by equations $\Phi_a = 0$ and $\Phi_b = 0$, respectively. At the apex of the pyramid, the six faces of the pyramid intersect and, hence, six normals can be defined. The plastic flow rule in this singular region

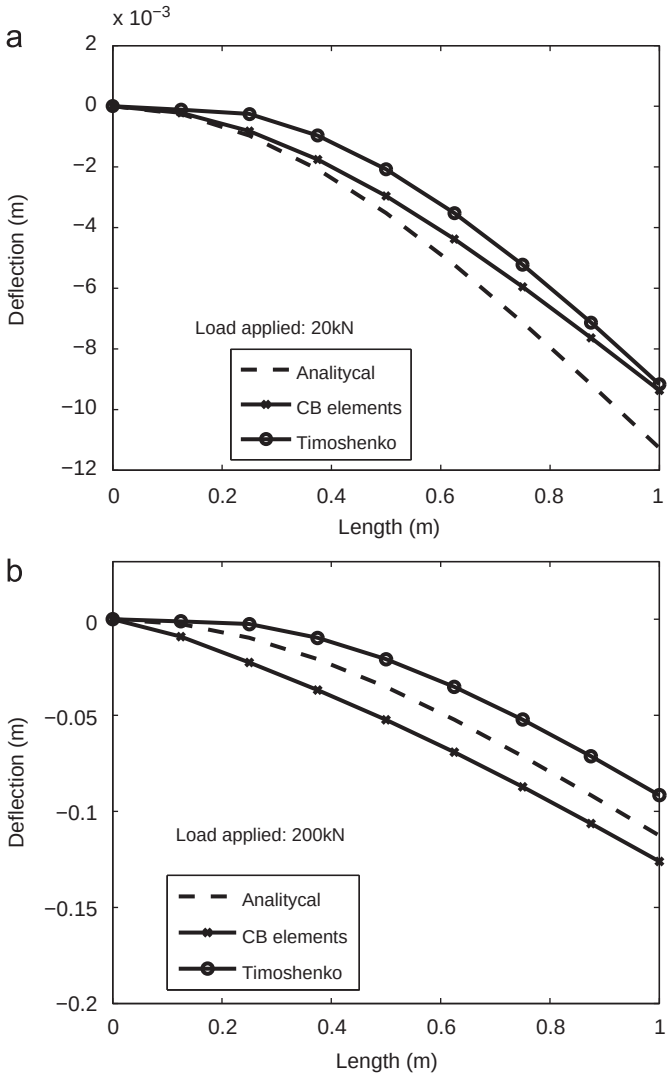

Fig. 7. Deflection along the cantilever for two different load tips. Comparisons are made against simulation by Timoshenko beam elements and analytical solution: (a) 20 kN; (b) 200 kN.

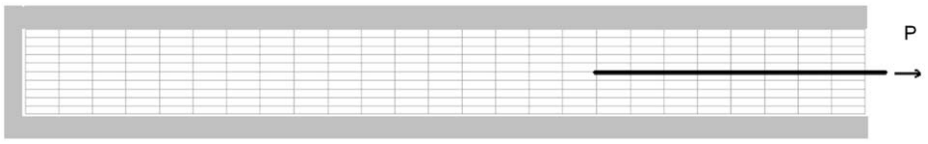

Fig. 8. Mesh and geometry of the tested pullout specimen.

Table 1
Material properties of the reinforced material.

	Block	Reinforcing bar
Young modulus (GPa)	14	180
Poisson's ratio	0.1	0.33
Yield stress (MPa)	30.5(t)/2.75(c)	300
Mass density (kg/m^3)	2400	7860
Friction angle (Φ)	20°	–
Dilatancy angle (Ψ)	20°	–

(t) and (c) denote *tension* and *compression* respectively.

is taken as a combination of these six normals, as follows:

$$\dot{\boldsymbol{\epsilon}}^p = \sum_{k=1}^{6} \mathbf{N}_k \tag{32}$$

It is interesting to remark that this associative plastic flow rule predicts a non-zero volumetric plastic strain, due to the pressure sensitivity of the Mohr–Coulomb criterion. The update of stress is performed in the principal stress space. Therefore, after performing the spectral decomposition of the trial elastic stress tensor, its eigencomponents can be arranged as

$$\sigma_{\mathrm{I}}^{trial} \geqslant \sigma_{\mathrm{II}}^{trial} \geqslant \sigma_{\mathrm{III}}^{trial}$$

Then, the possibility of yielding is checked with the consistency inequality,

$$\Phi^{trial} \equiv (\sigma_{\mathrm{I}}^{trial} - \sigma_{\mathrm{III}}^{trial}) + (\sigma_{\mathrm{I}}^{trial} + \sigma_{\mathrm{III}}^{trial}) \sin\phi \leqslant 2c(\bar{\varepsilon}_n^p)\cos\phi \tag{33}$$

where $\bar{\varepsilon}_n^p$ denotes the accumulated plastic strain. If inequality (33) is satisfied, then the step is purely elastic and the variables are directly

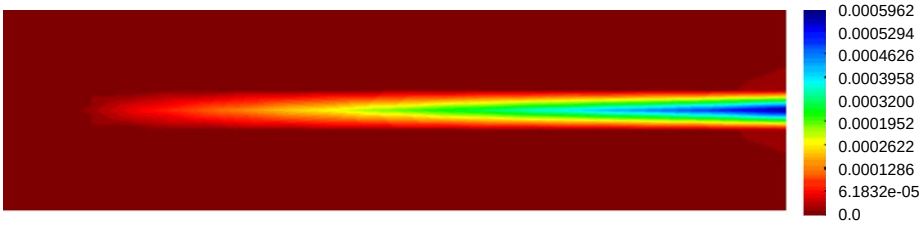

Fig. 9. Continuum—modelled as a softening material—from where the bar formed by CB is pulled out.

updated with the trial values. However, if inequality (33) is not satisfied, a plastic correction needs to be carried out. The general return mapping algorithm for the stress tensor is used to correct the value of stresses which lie on the softened yield surface,

$$\boldsymbol{\sigma} = \boldsymbol{\sigma}^{trial} - \mathbf{D}^e : \Delta\boldsymbol{\epsilon}^p \tag{34}$$

where $\mathbf{D}^e$ represents the elastic rate of deformation tensor. Taking into account the expressions (30)–(32), Eq. (34) can be re-written as

$$\boldsymbol{\sigma} = \boldsymbol{\sigma}^{trial} - \Delta\gamma\mathbf{D}^e : \mathbf{N} \tag{35}$$

References

[1] T. Belytschko, W.K. Liu, B. Moran, Nonlinear Finite Elements for Continua and Structures, Wiley, New York, 2001.
[2] K.J. Bathe, Finite Element Procedures, Prentice-Hall, Englewood Cliffs, NJ, 1996.
[3] O.C. Zienkiewicz, R.L. Taylor, The Finite Element Method: The Basis, vol. 1, fifth ed., Butterworth-Heinemann, Oxford, 2000.
[4] A. Cardona, M. Geradin, Beam finite element non-linear theory with finite rotations, Int. J. Numer. Methods Eng. 26 (11) (1988) 2403–2438.
[5] Z. Friedman, J.B. Kosmatka, An improved two-node Timoshenko beam finite element, Comput. Struct. 47 (3) (1993) 473–481.
[6] E. Spacone, V. Ciampi, F.C. Filippou, Mixed formulation of nonlinear beam finite element, Comput. Struct. 58(1) (1996) 71–83, 49 (1996) 55–70.
[7] E.N. Dvorkin, K.-J. Bathe, A continuum mechanics based four-node shell element for general nonlinear analysis, Eng. Comput. 1 (1984) 77–88.
[8] J.C. Simo, Finite strain beam theory, Comput. Methods Appl. Mech. Eng. 49 (1985) 55–70.
[9] Z.X. Li, A mixed co-rotational formulation of 2d beam element using vectorial rotational variables, Commun. Numer. Methods Eng. 23 (2007) 45–69.
[10] K.S. Kerkanen, J.T. Sopanen, A.M. Mikkola, A simple beam element for large rotation problems, Multi-Body Dynamics: Monitoring and Simulation Techniques-III, 2004, pp. 191–204.
[11] I.B. Edem, The exact two-node Timoshenko beam finite element using analytical bending and shear rotation interdependent shape functions, Int. J. Comput. Methods Eng. Sci. Mech. 7 (6) (2006) 425–431.
[12] E.L. Hill, Hamilton's principle and the conservation theorems of mathematical physics, Rev. Mod. Phys. 23 (3) (1951) 253–260.
[13] K.S. Kerkanen, J.T. Sopanen, A.M. Mikkola, A linear beam finite element based on the absolute nodal coordinate formulation, ASME J. Mech. Des. 127 (2005) 621–630.
[14] M.L. Bucalem, K.-J. Bathe, Locking behavior of isoparametric curved beam finite elements, Appl. Mech. Rev. 48 (1995) S25–S29.
[15] C.A. Felippa, B. Haugen, A unified formulation of small-strain corotational finite elements: I. Theory, Comput. Methods Appl. Mech. Eng. 194 (21–24) (2005) 2285–2335.
[16] K.M. Hsiao, Corotational total Lagrangian formulation for three-dimensional beam element, AIAA J. 30 (3) (1992) 797–804.
[17] Y. Urthaler, J.N. Reddy, A corotational finite element formulation for the analysis of planar beams, Commun. Numer. Methods Eng. 21 (10) (2005) 553–570.
[18] J.L. Curiel Sosa, E.A. de Souza Neto, D.R.J. Owen, A combined implicit–explicit algorithm in time for non-linear finite element analysis, Commun. Numer. Methods Eng. 22 (2006) 63–75.
[19] J.L. Curiel Sosa, Computational modelling of critical points and structural discontinuities. Ph.D. Thesis, Civil and Computational Engineering Centre, Swansea University, Singleton Park, Swansea, UK, 2006.
[20] G. Prathap, G.R. Bhashyam, Reduced integration and the shear-flexible beam element, Int. J. Numer. Methods Eng. 18 (2) (1982) 195–210.
[21] O.C. Zienkiewicz, R.L. Taylor, The Finite Element Method: Solid Mechanics, vol. 2, fifth ed., Butterworth-Heinemann, Oxford, 2000.
[22] A. Munjiza, D.R.J. Owen, A.J.L. Crook, An $M\cdot(M^{-1}K)^m$ proportional damping in explicit integration of dynamic structural systems, Int. J. Numer. Methods Eng. 41 (1998) 1277–1296.
[23] T. Belytschko, T.J.R. Hughes, Computational Methods for Transient Analysis, Elsevier Science, The Netherlands, 2001.
[24] J.C. Simo, T.R. Taylor, Return mapping algorithm for plane stress elastoplasticity, Int. J. Numer. Methods Eng. 22 (1986) 649–670.
[25] I.M. May, C.T. Morley, Y.Y. Chen, Benchmarking of non-linear finite element analyses for reinforced concrete deep beams, in: N. Bicanic, R. de Borst, H. Mang, G. Meschke (Eds.), Proceedings of the Euro-C, Conference on Computational Modelling of Concrete Structures, Mayrhofen, Tyrol, Austria, A A Balkema Publishers, 2003.
[26] J.C. Simo, T.J.R. Hughes, Computational Inelasticity, Springer, Berlin, 1998.